On the Probability Density Function and Stability Properties for a Cross-Product Frequency-Locked Loop

Tsung-Yu Chiou
Stanford University, Palo Alto, California

BIOGRAPHY

Tsung-Yu Chiou is a Ph.D. candidate in the Aeronautics and Astronautics Department at Stanford University. He received his B.S. in Aerospace Engineering in 1998 from Tamkang University, Taiwan and his M.S. from Stanford in 2002. His research currently focuses on the performance analysis and validation of Inertial-aided GPS carrier-tracking loops. He is also looking into the solutions to the problem of GPS/WAAS performance degradation caused by ionospheric scintillation.

ABSTRACT

The frequency locked-loop (FLL) has received new attention for modern Global Navigation Satellite Systems (GNSS) receivers, especially for its performance under severe noise interference and high dynamic environments. It has been shown that an FLL is more robust to interference and dynamics than a phase locked-loop (PLL). Therefore, it is beneficial to use an FLL as a fallback tracking loop when the primary PLL is unable to maintain carrier tracking in hostile environments. Besides tracking, it is to also crucial to preserve the Bit Error Rate (BER) of the data demodulation and probability of losing locks when receivers operate an FLL. These characteristics rely on the probability density function (PDF) of the frequency estimate made by the frequency discriminator in the FLL. However, the PDF has not been determined as of yet. The purpose of this paper is to solve the PDF and evaluate the stability region, which is essential for determining the statistics of loss of lock. In this work, a nonlinear model was developed and the corresponding Fokker-Planck equation (FPE) for the cross-product FLL was derived. The PDF of the frequency estimate was then solved by applying the Crank-Nicolson numerical method.

I. INTRODUCTION

The use of a frequency-locked loop (FLL) can be traced back to the 1930s [1], while an FLL used to be called an automatic frequency control (AFC) loop. The function of an FLL in a GNSS receiver is to steer the frequency of the replica carrier close enough to the frequency of the received carrier such that a further data demodulation is applicable. In stead of a coherent tracking, meaning that the signal phase is tracked by a phase-locked loop (PLL), an FLL performs a non-coherent tracking only. For example, only the frequency in the carrier is tracked while assuming that the phase is uniformly distributed over [0, 2π]. Thus, an FLL can pull in from a frequency error much larger than a PLL does. It is believed that an FLL is more robust in the presence of noise interference under high dynamic environments than a PLL [2]. The applications of an FLL generally can be divided in two categories, in which an FLL can be used to improve the initial tracking of a PLL [4] or used as a backup tracking loop when the received signal power is weak during a short period [5]. Hence, investigating the performance of an FLL used in a GNSS receiver is significant and important.

Research on the linear model analysis of various types of FLL's has already been accomplished [2, 3]. The noise performance of the FLL in the presence of Gaussian noise has been given in [2, 3]. However, the probability density function (PDF) of an FLL has not been solved. Obtaining the PDF is crucial to evaluate the bit error rate (BER) in the demodulation process. Moreover, estimating the probability of losing lock also relies on the PDF of the FLL.

The objective of the present paper is to develop the nonlinear model of the cross-product FLL, evaluate the nonlinear stability characteristics in the absence of noise, and solve for the PDF in the presence of noise.

II. BASIC OPERATION OF THE CROSS-PRODUCT FLL

In this section, I would like to review the operation of the cross-product FLL without giving details of the mathematical derivation. For the details, references [2, 3] are recommended. Figure 1 shows the configuration of the cross-product FLL. The essential characteristic of this FLL is the fact that it employs a cross-product frequency discriminator, which is a conventional FLL design in modern digital baseband implementation [2]. Except the cross-product discriminator, the functionality shown in Figure 1 is the well known Costas receiver [6]. The input signal, $V_s(t)$, is assumed to be a carrier, at frequency ω_0, modulated with differentially encoded data and pluses an additive white Gaussian noise with spectral density $N_0/2$. $V_s(t)$ is then multiplied by the local replica carrier, at frequency ω_1, generated by the numerically controlled oscillator (NCO). The multiplications were performed by the in-phase and quadrature replica carrier to produce I and Q channels, respectively. The I and Q channels are then passed through the integrate-and-dump filters to further reject the input noise prior to performing the frequency error determination in the following step. Before the details of the frequency discriminator, we define a complex signal composed by the outputs of the integrate-and-dump filters, I_k and Q_k, as the following form

$$\overline{V_s}(k) = I_k + jQ_k \,. \tag{1}$$

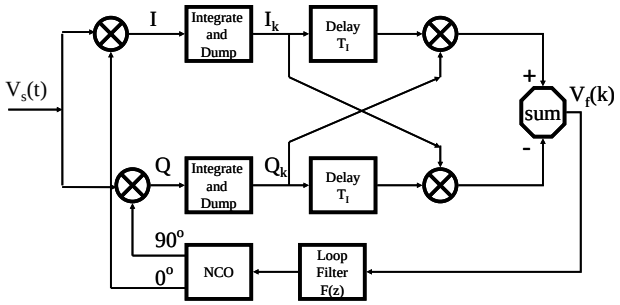

Figure 1: Cross Product FLL

The operation of the cross-product frequency discriminator is the cross product of the current sample of $\overline{V_s}(k)$ and the previous sample of $\overline{V_s}(k)$. This operation is represented as [3]

$$\begin{aligned} V_f(k) &= \overline{V_s}(k) \times \overline{V_s}(k-1) = I_{k-1}Q_k - Q_{k-1}I_k \\ &= d_k d_{k-1} A^2 \mathrm{sinc}^2\left(\frac{\Delta\omega T_I}{2}\right) \cdot \sin(\Delta\omega T_I) + N(k) \end{aligned}, \tag{2}$$

where

d_k is the data symbol at the k th integrate-and-dump step;

A is signal amplitude;

$\Delta\omega = \omega_0 - \omega_1$;

T_I is the period of the integration;

$\mathrm{sinc}(x) = \dfrac{\sin(x)}{x}$;

$N(k)$ is the noise term.

Obviously, the sign of $V_f(k)$ depends on the sign of the symbol product $d_k d_{k-1}$. The sign changes can be removed by performing the dot product of current sample $\overline{V_s}(k)$ and the previous sample of $\overline{V_s}(k)$ [2, 3]. The output of the dot product is then used as a decision feedback to remove the sign changes in Eq. (2). Here, we assume that the data has been wiped off by the means of dot product operation. This assumption is reasonable since we are solving for the generic performance of a carrier tracking loop. Without loss of generalities, one can further assume that the input signal is a pure sinusoidal carrier. The plot of the frequency discriminator assuming noise free is shown in Figure 2. Note that the frequency error shown in Figure 2 has been normalized by multiplying Δf by the integration time T_I.

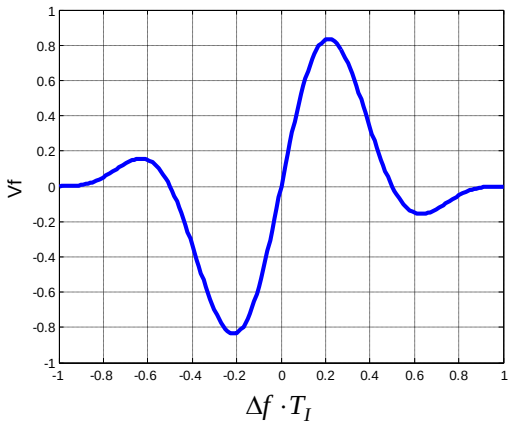

Figure 2: Cross Product FLL discriminator curve

From Figure 2, we see that unlike the periodic property of the phase discriminator in a PLL [8], there is no exact periodicity in the frequency discriminator. The main lock point is at the origin. Once the frequency error deviates far away from the first zero crossing point, the loop likely starts to lose lock. As can be seen in Figure 2, the characteristic of the discriminator is close to linear when the value $\Delta f \cdot T_I$ is small. A rule-of-thumb threshold to preserve this linearity assumption is when [7]

$$\Delta f \cdot T_I \le \frac{1}{12} \cong 0.083 \,. \tag{3}$$

Although the input signal is corrupted by the Gaussian noise, $N(k)$ in Eq. (2), in fact, is not a Gaussian distributed noise because of the nonlinear process of the discriminator. It is shown that $N(k)$ is zero mean and uncorrelated in successive samples [3]. To advance the model analysis, one usually assumes that $N(k)$ is Gaussian. As a result, given that the noise at the input signal is white Gaussian noise with two-sided spectral density $N_0/2$ and the pre-detection baseband bandwidth $1/T_I$, one can obtain the mean, variance or the second moment, and power spectral density (PSD) of $N(k)$ as follows [3].

$$E[N(k)] = 0. \tag{4}$$

$$E[N^2(k)] = \frac{2N_0^2}{T_I}\left[\frac{2C}{N_0} + \frac{1}{T_I}\right]. \tag{5}$$

$$S_N(f) = N_0^2\left[\frac{2C}{N_0} + \frac{1}{T_I}\right] \text{ (two-sided)}, \tag{6}$$

where C/N_0 is the signal power to noise power density ratio.

With the assumption of Eq. (3), a spectral analysis can be performed in the linear model of the FLL. Thus, the normalized tracking error variance of the cross-product FLL is ([9], page 381)

$$\sigma^2_{\Delta f T_I} = \frac{1}{4\pi^2}\frac{4B_n}{\frac{C}{N_0}}\left[1 + \frac{1}{2T_I\frac{C}{N_0}}\right], \text{ dimensionless}^2 \tag{7}$$

where B_n, in Hz, is the one-sided noise bandwidth of the closed loop FLL.

III. NONLINEAR MODEL AND THE STABILITY OF THE FLL IN THE ABSENCE OF NOISE

III-1. NONLINEAR MODEL

Given the block diagram in Figure 1 and the characteristic of the cross-product discriminator in Eq. (2), the nonlinear model representing the cross-product FLL is shown in Figure 3. The additive noise $N(t)$ has the properties described in Eqs. (4-6).

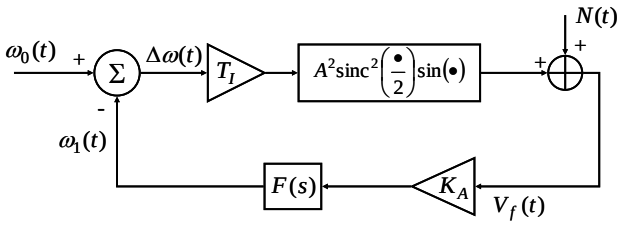

Figure 3: Nonlinear Model of the Cross Product FLL

$F(s)$ is the loop filter represented in the Laplace domain and K_A is the loop gain. Note that the carrier NCO in an FLL does not act as an integrator. It is simply a means of converting a frequency number to sine and cosine of frequency ([9], page 384). Therefore, the order of the closed-loop is the same as the order of the loop filter.

For a nonlinear analysis, investigating the performance of the first order loop suffices the required characteristics of the FLL. Therefore, in the first order loop, $F(s) = 1/s$. We can obtain the following state equation describing the closed loop shown in Figure 3 as the following equation.

$$\frac{d\Delta\omega(t)}{dt} = \frac{d\omega_0(t)}{dt} - A^2K_A\text{sinc}^2\left(\frac{\Delta\omega(t)T_I}{2}\right)\sin\left(\Delta\omega(t)T_I\right) - K_AN(t). \tag{8}$$

We consider primarily frequency-ramp sinusoidal inputs, so that $d\omega_0(t)/dt = \nu$, which is a constant in units of rad/sec^2. If ν is zero, we say that loop is unstressed. In the unstressed case, the distribution of the tracking error would be zero mean. If ν is nonzero, the FLL is dynamically stressed and the mean of the tracking error would be biased from zero. Let $z = \Delta f \cdot T_I$ and we have

$$\Delta\omega = \frac{2\pi}{T_I}z \text{ and } d\Delta\omega = \frac{2\pi}{T_I}dz.$$

Perform the change of variables in $\Delta\omega$ and z for Eq. (8), we have the following governing equation of the cross-product FLL in the domain of the normalized frequency error.

$$\frac{dz(t)}{dt} = \frac{T_I}{2\pi}\left[\nu - A^2K_A\text{sinc}^2(\pi z)\sin(2\pi z) - K_AN(t)\right]. \tag{9}$$

Eq. (9) is a stochastic first order ordinary differential equation which fully describes the behavior of the cross-product FLL. The solution of $z(t)$ in Eq. (9) is of interest. In the next section, we will show the statistical solution to

Eq. (9). In the rest of this section, I would like to discuss the stability performance in the absence of noise, which is essential to obtain the boundary of z where the FLL loses lock.

III-2. THE STABILITY OF THE FLL IN THE ABSENCE OF NOISE

I investigate the system trajectory described in Eq. (9) without considering the noise term $N(t)$. For the first order loop, the loop noise bandwidth is [9]

$$B_n = \frac{A^2 K_A}{4}. \tag{10}$$

The input frequency ramp ν can be written as

$$\nu = 2\pi \dot{\Delta f}_i, \tag{11}$$

where $\dot{\Delta f}_i$ is the frequency ramp input in $^{Hz}/_{\sec}$.

Substitute Eqs. (10) and (11) into Eq. (9) with ignoring the noise term, we have

$$\frac{dz(t)}{dt} = \left[\dot{\Delta f}_i T_I - \frac{4B_n T_I}{2\pi} \operatorname{sinc}^2(\pi z) \sin(2\pi z) \right]. \tag{12}$$

The system trajectory of Eq. (12) is shown in Figure 4 for the case of an unstressed FLL. One can find that the system is stable when it reaches a value of z for which $^{dz}/_{dt} = 0$. There are multiple stable points for the system. However, the FLL is allowed to be locked only within the main lobe for a physical means of tracking. One can find that the system moves toward the right when $^{dz}/_{dt} > 0$ and vice versa. Therefore, there are dynamically stable points for z = …-1,0,1,2…, where the system will return to the stable points after any perturbation of z in either direction. However, for other stables points, any perturbation of z in either direction will cause the system to move until it reaches the next dynamically stable point.

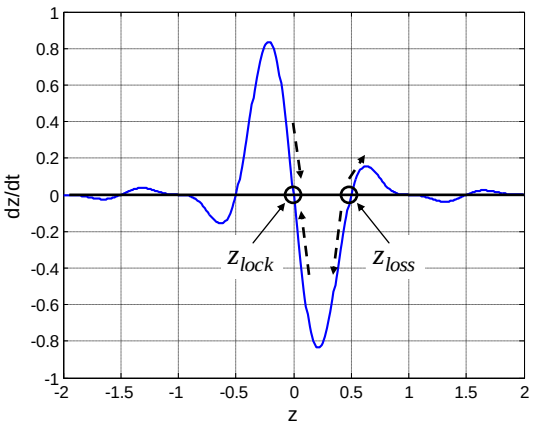

Figure 4: System Trajectory, Non-stressed

$$\dot{\Delta f}_i T_I = 0, \quad T_I = 1, \quad 4B_n = 2\pi$$

We call the dynamically stable point in the main lobe z_{lock} and the next non-dynamically stable point z_{loss}. Once z is larger than z_{loss}, the system moves farther away from the main lobe and stops when it reaches the next stable point. However, when the system is dynamically stressed, there may be no stable points beyond z_{loss}. Figure 5 illustrates the issue of having only two stable points.

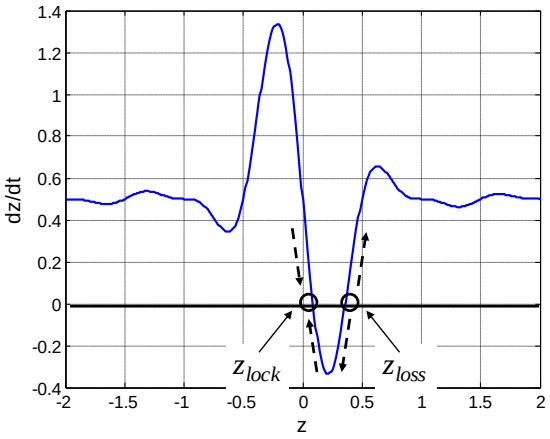

Figure 5: System Trajectory, Dynamically Stressed

$$\dot{\Delta f}_i T_I = 0.5, \quad T_I = 1, \quad 4B_n = 2\pi$$

With a positive frequency ramp input, one can find that once $z > z_{loss}$, the system will migrate toward infinity and never returns to any stable points. Thus z_{loss} is the threshold where the FLL starts to lose lock. If the input frequency ramp increases again, the whole curve shifts upward such that z_{lock} and z_{loss} move further toward each other. This means that the FLL is more likely to lose lock under stronger dynamics. The frequency ramp for the

case that z_{lock} and z_{loss} coincide is the maximum allowable frequency ramp for the first order FLL. Any input beyond the maximum allowable ramp frequency will cause the FLL to be unstable.

Knowing the values of z_{loss} is crucial for evaluating the probability of loss of lock in the presence of noise. The probability of loss of lock is defined as

$$P\left(z > z_{loss} \mid B_n, \dot{\Delta f_i}\, T_I \right). \tag{13}$$

Determining the value of Eq. (13) relies on the PDF of z, which will be provided in the next section.

IV. THE FOKKER-PLANCK EQUATION AND THE PDF OF THE CROSS-PRODUCT FLL

In this section, a statistical approach to Eq. (9) will be discussed. Eq. (9) is a stochastic ordinary differential equation driven by a Gaussian noise $N(t)$. Therefore, given $z(t)$, the PDF of dz/dt is Gaussian too. As a result, the complete solution of $z(t)$ is determined by its PDF.

Since $N(t)$ is Gaussian, the process described in Eq. (9) is a Markov process and the relations governing a PDF of a Markov process is given by [8]

$$\frac{\partial p(z,t)}{\partial t} = \sum_{n=1}^{\infty} \frac{(-1)^n}{n!} \frac{\partial^n}{\partial z^n} \left[A_n(z)\, p(z,t) \right] \tag{14}$$

with initial condition

$$p(z,0) = \delta(z - z_0),$$

where

$p(z,t)$ is the PDF of $z(t)$;
$A_n(z)$ = the limit of the nth moment of the increment of the process Δz, given that it started at some value z at time t, normalized by the time increment Δt as the latter approaches zero;
$\delta(z - z_0)$ is Dirac delta function.

It is known that for a first-order stochastic ordinary differential equation with a white Gaussian driving function, the quantities $A_n(z)$ vanish for n greater than 2 [8]. Accordingly, Eq. (14) becomes the well known Fokker-Planck equation (FPE) as follows

$$\begin{aligned} &\frac{\partial p(z,t)}{\partial t} = -\frac{\partial}{\partial z}\left[A_1(z)\, p(z,t) \right] + \frac{1}{2}\frac{\partial^2}{\partial z^2}\left[A_2(z)\, p(z,t) \right] \\ &p(z,0) = \delta(z - z_0) \end{aligned} \tag{15}$$

In order to obtain the corresponding FPE for the cross-product FLL, we must determine the quantities $A_1(z)$ and $A_2(z)$ according to Eq. (9). The derivation is given in the Appendix A and, $A_1(z)$ and $A_2(z)$ are given in Eqs. (A-3) and (A-4), respectively. In addition to the initial condition given in Eq. (15), solving the FPE needs two boundary conditions. We know that the total area under a PDF should be 1 and accordingly the two tails of the PDF approach zero as the independent variable approaches plus and minus infinities. The two boundary conditions are then defined as follows.

The normalization condition is

$$\int_{-\infty}^{\infty} p(z,t)\, dz = 1, \text{ and} \tag{16}$$

the symmetric condition is

$$p(\infty,t) = p(-\infty,t) = 0, \text{ for all } t. \tag{17}$$

Note that the symmetric condition is a heritage of the normalized condition since the total area has to be finite and therefore the two tails have to vanish at infinities.

To further advance the solution of the FPE, we would like to parameterize the FPE in terms of B_n, C/N_0, T_I, normalized initial frequency offset $\Delta f_i T_I$, and normalized frequency ramp input $\dot{\Delta f}_i T_I$. Eq. (18) gives the expression of the final FPE to be solved. The details for obtaining Eq. (18) are given in Appendix B.

$$\begin{aligned} &\frac{\partial p(z,t)}{\partial t} = \eta\left\{ -\frac{\partial}{\partial z}\left[D(z)\, p(z,t) \right] + \frac{1}{2}\frac{\partial^2}{\partial z^2}\, p(z,t) \right\}; \\ &p(z,0) = \delta(z - z_0); \\ &\int_{-\infty}^{\infty} p(z,t)\, dz = 1; \\ &p(\infty,t) = p(-\infty,t) = 0, \end{aligned} \tag{18}$$

where
$z = \Delta f \cdot T_I$, the normalized frequency error;
$p(z,t)$ = the PDF of the FLL in the domain of the normalized frequency error;
$\eta = 2T_I^2 \cdot B_n \cdot \sigma^2_{\Delta f T_I}$;

$$D(z) = \frac{2\pi}{T_I}\left[\beta - \alpha \mathrm{sinc}^2(\pi z)\sin(2\pi z)\right];$$

$$\alpha = \frac{1}{2\pi^2 \sigma^2_{\Delta f T_I}};$$

$$\beta = \alpha \cdot \frac{2\pi}{T_I}\gamma_z;$$

$\gamma_z = \frac{\dot{\Delta f_i} T_I}{4B_n}$, the dimensionless dynamic stress;

$z_0 = \Delta f_i \cdot T_I$, the normalized initial frequency offset.

Because of the nonlinearity of the discriminator (shown in the term $D(z)$), the closed form representation of the steady state PDF is not achievable yet. A numerical method to solve the FPE will be discussed in the next section.

V. NUMERICAL RESULTS BY THE CRANK-NICOLSON METHOD

To solve the partial differential equation of Eq. (18), I conducted the Crank-Nicolson method [10]. The corresponding difference equation to Eq. (18) is therefore

$$\frac{p_i^{j+1} - p_i^j}{\Delta t} = \frac{1}{2}\eta \cdot \left\{\left[-\frac{D(z_{i+1})p_{i+1}^j - D(z_{i-1})p_{i-1}^j}{2\Delta z} + \frac{1}{2}\frac{p_{i+1}^j - 2p_i^j + p_{i-1}^j}{(\Delta z)^2}\right] + \left[-\frac{D(z_{i+1})p_{i+1}^{j+1} - D(z_{i-1})p_{i-1}^{j+1}}{2\Delta z} + \frac{1}{2}\frac{p_{i+1}^{j+1} - 2p_i^{j+1} + p_{i-1}^{j+1}}{(\Delta z)^2}\right]\right\}, \quad (19)$$

where the subscripts, i ,denote spatial domain of z and the superscripts, j, denote time. Note that $D(z)$ is time independent and there is no superscript for $D(z)$. Figure 6 shows the time and spatial meshes for Eq. (19). Given $p(z_i, t_j)$ at time t_j, solving Eq. (19) will give the PDF at time t_{j+1} for all z_j. The initial condition for the numerical solution is the Kronecker delta function, which satisfies both of the normalized condition and the boundary conditions at the initial state. The symmetric boundary condition is approximated by using an absorbing boundary condition. It is reasonable to assume that the tails of the PDF approach zero within a finite range of z. Once the accuracy of the solution is met given an absorbing boundary condition, the solution was claimed to be valid. The aforementioned accuracy was calculated from the difference of the total area under the solved PDF to 1. In other words, the normalized boundary condition is used as a metric for claiming a successful solution. In this paper, the accuracy requirement was set to be 1e-12. The number of the grids in z direction was 7000 or more. Intuitively, as more grids used for the mesh, more accurate results will be. However, the amount of memory on the computer limits the grid number. The required number of grids also depends on C/N_0. As expected, the PDF for a lower C/N_0 has a wider range in z direction. Therefore, to preserve the required accuracy, more grids are needed to cover the wider range of z. The time step size also depends on the grid size in z. The details of the trade off between the grid size in z and the time step size are given in [10].

For calculations of $D(z)$, one should know that the definition of the sinc function in Matlab differs from what was defined in Eq. (2). In Matlab, the sinc function is defined

$$\mathrm{sinc}(x) = \frac{\sin(\pi x)}{\pi x}.$$

Figure 7 shows one example of the PDF solution. In Figure 7, there is an initial frequency offset assumed. The initial impulse is at $z = 0.05$. The green curve represents the PDF at the half of the evolving time and the red curve is the PDF at the end of the evolving time. The coinciding of the green and red curves shows that the FLL has reached the steady state. Figure 7 also shows that the steady state error is zero as expected for the performance of a first order loop with an initial impulse input.

Figure 8 shows another example for the case that the PDF is dynamically stressed. The final PDF is centered at the steady state value of the frequency error.

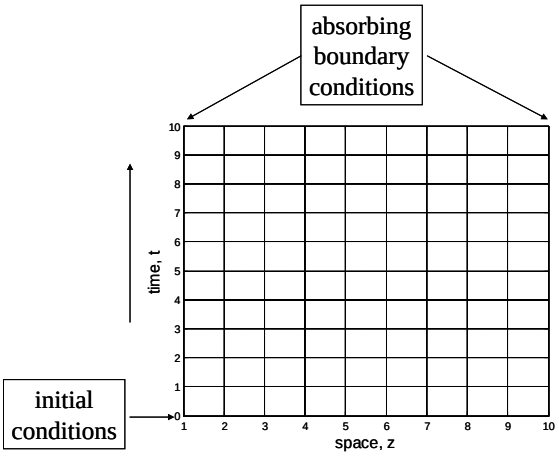

Figure 6: The time and spatial meshes for numerical solution of FPE

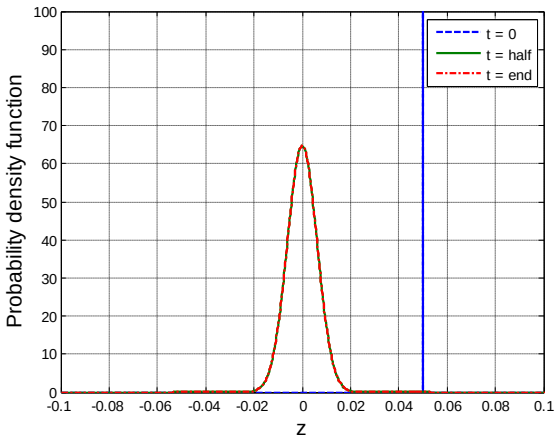

Figure 7: PDF of the FLL, Non-stressed

$C/N_0 = 20dB-Hz, B_n = 10Hz, \Delta f_i T_I = 0.05, \dot{\Delta f_i} T_I = 0$

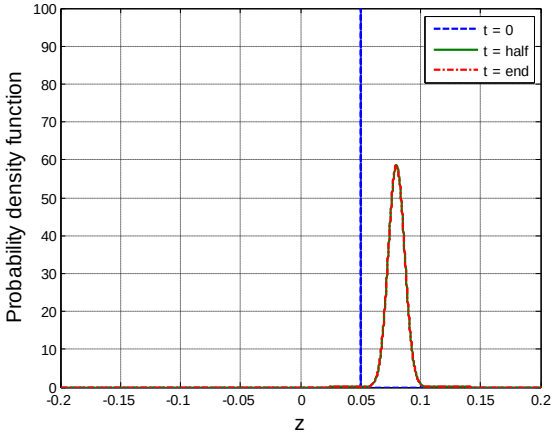

Figure 8: PDF of the FLL, Dynamically-stressed

$C/N_0 = 20dB-Hz, B_n = 10Hz, \Delta f_i T_I = 0.05, \dot{\Delta f_i} T_I = 3Hz$

VI. DISCUSSIONS

One may not obviously see the correlation between the system trajectory, shown in Figure 4, and the PDF, shown in Figure 7. To illustrate this correlation, a PDF with C/N_0 = 0 dB-Hz is plotted in Figure 9. From the case of weak signal shown in Figure 9, we see two deeps in the PDF for $|z|$ = 0.5. This, again, reveals the fact that the z_{loss} points in Figure 4 are not dynamically stable points. The system has the lowest possibility to stay at these two points. The wavelet behavior in Figure 9 also represents the same behavior in Figure 4. The system has relative lower possibilities, comparing to its adjacent points, to stay at those non-dynamically stable points.

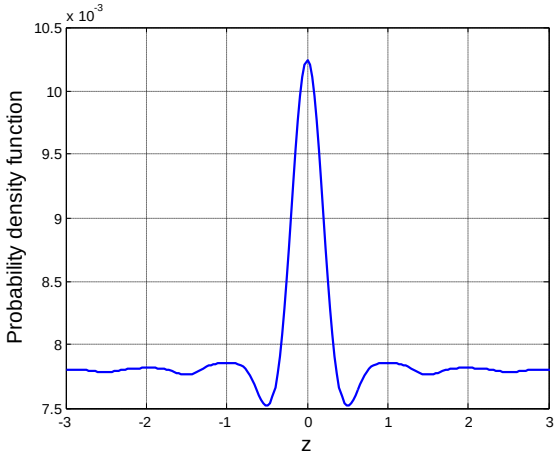

Figure 9: PDF of the FLL, Weak Signal

$C/N_0 = 0dB-Hz, B_n = 10Hz, \Delta f_i T_I = 0, \dot{\Delta f_i} T_I = 0Hz$

Since there is a steady state solution of the PDF for the FLL, we can eliminate the time dependence of the PDF in Eq. (18). On the other hand, the left hand side of Eq. (18) becomes zero and the PDF on the right hand side of Eq. (18) does not have the variable t. As a result, Eq. (18) becomes a second order nonlinear ordinary differential equation (ODE) shown in Eq. (20).

$$0 = -\frac{\partial}{\partial z}\left[D(z)p(z)\right] + \frac{1}{2}\frac{\partial^2}{\partial z^2}p(z);$$
$$\int_{-\infty}^{\infty} p(z)dz = 1; \qquad (20)$$
$$p(\infty) = p(-\infty) = 0$$

The solution of Eq. (20) is the final snapshot of the time-dependent solutions obtained from solving Eq. (18). A simple finite difference method was applied to solve Eq. (20) for the steady state PDF. Figure 10 shows the solutions from both of the ODE (Eq.(20)) and the PDE (Eq.(18)). The solution of the ODE further verified the solution of the PDE. Therefore, it is true that the steady state PDF of the FLL can be directly solved from the ODE in Eq. (20) without solving the PDE in Eq. (18) by the Crank-Nicolson method. However, without the process of investigating the solution of the PDE, we can not conclude the fact that the steady state solution exists. If one is interested in the steady state PDF of the FLL, one can directly solve the ODE in Eq. (20). However, if the transient properties are of interest, solving the PDE is necessary.

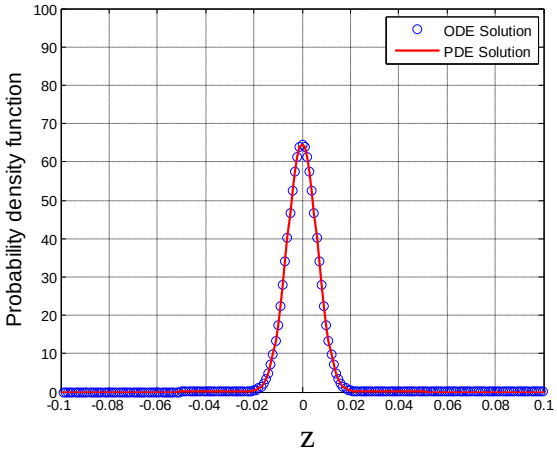

Figure 10: PDF of the FLL, ODE and PDE Solutions

$C/N_0 = 20dB-Hz, B_n = 10Hz, \Delta f_i T_I = 0, \dot{\Delta f_i} T_I = 0Hz$

Once the PDF of the FLL is available, one can, for example, estimate the probability of exceeding the linear threshold given in Eq. (3). Figure 11 shows the curve of this probability versus different C/N_0 with fixed noise bandwidth and the integration time. The curve was obtained by calculating the tail area of the PDF beyond the linear threshold defined in Eq. (3) for the FLL. Figure 11 also shows the probability for a Costas PLL. Since the PDF of the PLL has been solved [8, 11], this probability can be evaluated by using the closed form solution. Note that the PDF of the PLL given in [8, 11] must be modified to account for the use of a Costas loop. The modified PDF of the PLL can be found in [5] or ([12], page 274). The linear threshold of the PLL was set to be 15 degrees [7]. Therefore, the red curve in Figure 11 was the tail area beyond the 15 degree threshold. Note that the phase error variance used in the PDF of the PLL considered only the thermal noise without a squaring loss term ([13], page 290) but not considered the phase error variance with the squaring loss term ([9], page 371).

As seen in Figure 11, the probability of exceeding the linear threshold for the FLL is smaller than that for the Costas PLL. Figure 11 suggests that if the PLL does not maintain lock due to low C/N_0, one may switch to use FLL with accuracy degradations in carrier measurements. Figure 11 emphasizes the relative difference between the two tracking loops but not the absolute values read from the figure. The reason is that the curves in Figure 11 considered tracking error due to thermal noise only. However, the tracking error is also affected by receiver clock dynamics, satellite clock dynamics, platform vibration impacts on the local oscillator and the acceleration sensitivity of the local oscillator [5]. With considering all of the above error sources given the same noise bandwidth, integration time and C/N_0, the actual probability of exceeding the linear threshold would be larger than what it is shown in Figure 11.

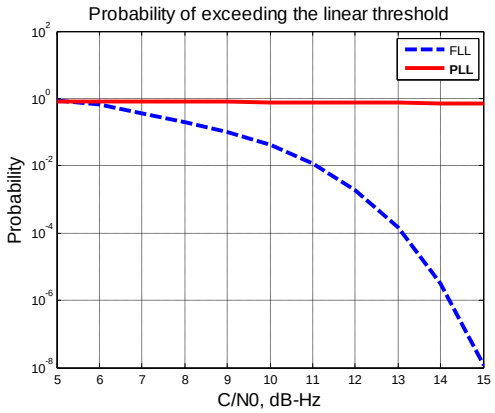

Figure 11: Probability of Exceeding the Linear Threshold

$B_n = 10Hz, T_I = 0.01\text{sec}$

VII. CONCLUSIONS

The nonlinear model of the cross-product FLL has been developed and the stability analysis as well as the PDF for the FLL has been solved for the first time. The PDF of the FLL was solved numerically in both PDE and ODE approaches. With the PDF, one can estimate a more accurate Bit Error Rate (BER) due to imperfect frequency estimating of the FLL. Given the system trajectories of z_{lock} and z_{loss} shown in Figure 4, 5 and the solution of the Fokker-Planck equation, one can estimate the probability of loss of lock defined in Eq. (13).

In conclusion, this paper successfully solves the probability density function of the cross-product FLL and provides the stability analysis for evaluating the probability of loss of lock for a GNSS receiver using the FLL.

ACKNOWLEDGMENTS

The author gratefully acknowledges the sponsor of this research at Stanford University, the FAA satellite navigation product team.

I am also sincerely grateful to Dr. Francis Natali for his advice on this paper and especially for his comprehensive comments on the analysis of the frequency-locked loop. Special thanks to Professor Per Enge and Dr. Todd Walter of Stanford University for their knowledgeable commentary on the analysis of this paper. For Jen-Der Lee in the Aerospace Computing Lab at Stanford University, much appreciation is due for his constructive comments and advice on the numerical approach to a partial differential equation.

APPENDIX A

From the definition of $A_n(z)$ in Eq. (14), the expression of $A_n(z)$ can be written as [8]

$$\begin{aligned} A_n(z) &= \lim_{\Delta t\to 0}\frac{1}{\Delta t}\int_{-\infty}^{\infty}(\Delta z)^n\, p(\Delta z \mid z)d(\Delta z) \\ &= \lim_{\Delta t\to 0}\frac{E\left[(\Delta z)^n \mid z\right]}{\Delta t} \end{aligned} \tag{A-1}$$

By integrating both sides of Eq. (9) over the infinitesimal interval from t to $t+\Delta t$, we have

$$\begin{aligned} &\Delta z = z(t+\Delta t) - z(t) \\ &= \frac{T_I}{2\pi}\left[\nu - A^2K_A\,\mathrm{sinc}^2(\pi z)\sin(2\pi z)\right]\Delta t - \frac{T_I}{2\pi}K_A\int_t^{t+\Delta t}N(t)dt \end{aligned} \tag{A-2}$$

Recalling that $N(t)$ is white Gaussian noise of zero mean and the two-sided spectral density given in Eq. (6), we find that the first two normalized moments of Eq. (A-1) are

$$\begin{aligned} A_1(z) &= \lim_{\Delta t\to 0}\frac{E\left[(\Delta z) \mid z\right]}{\Delta t} \\ &= \frac{T_I}{2\pi}\left[\nu - A^2K_A\,\mathrm{sinc}^2(\pi z)\sin(2\pi z)\right] \end{aligned} \tag{A-3}$$

$$\begin{aligned} A_2(z) &= \lim_{\Delta t\to 0}\frac{E\left[(\Delta z)^2 \mid z\right]}{\Delta t} \\ &= \lim_{\Delta t\to 0}\left(\frac{T_I}{2\pi}\right)^2\frac{K_A^2}{\Delta t}\int_t^{t+\Delta t}\int_t^{t+\Delta t}E\left[N(u)N(v)\right]dudv \\ &= \lim_{\Delta t\to 0}\left(\frac{T_I}{2\pi}\right)^2\frac{K_A^2}{\Delta t}N_0^2\left[\frac{2C}{N_0}+\frac{1}{T_I}\right]\int_t^{t+\Delta t}\int_t^{t+\Delta t}\delta(u-v)dudv \\ &= \left(\frac{T_I}{2\pi}\right)^2K_A^2N_0^2\left[\frac{2C}{N_0}+\frac{1}{T_I}\right] \end{aligned} \tag{A-4}$$

APPENDIX B

Rewrite Eq. (15)

$$\begin{aligned} &\frac{\partial p(z,t)}{\partial t} = -\frac{\partial}{\partial z}\left[A_1(z)\,p(z,t)\right] + \frac{1}{2}\frac{\partial^2}{\partial z^2}\left[A_2(z)\,p(z,t)\right], \\ &p(z,0) = \delta(z-z_0) \end{aligned} \tag{B-1}$$

where $A_1(z)$ and $A_2(z)$ are given in Eqs. (A-3) and (A-4).

Let $\eta = A_2(z)$. Given the one-sided noise bandwidth in Eq. (10) and the variance of the normalized frequency error in Eq. (7), we can find that

$$\eta = 2T_I^2\cdot B_n\cdot\sigma_{\Delta fT_I}^2. \tag{B-2}$$

Define

$$\alpha = \frac{A^2K_A}{K_A^2N_0^2\left[\frac{2C}{N_0}+\frac{1}{T_I}\right]} \text{ and } \beta = \frac{\nu}{K_A^2N_0^2\left[\frac{2C}{N_0}+\frac{1}{T_I}\right]}.$$

Eq. (B-1), then, can be written as

$$\begin{aligned} &\frac{\partial p(z,t)}{\partial t} = \eta\left\{-\frac{\partial}{\partial z}\left[D(z)\,p(z,t)\right] + \frac{1}{2}\frac{\partial^2}{\partial z^2}\,p(z,t)\right\}; \\ &p(z,0) = \delta(z-z_0); \\ &\int_{-\infty}^{\infty}p(z,t)dz = 1; \\ &p(\infty,t) = p(-\infty,t) = 0, \end{aligned} \tag{B-3}$$

where

$$D(z) = \frac{2\pi}{T_I}\left[\beta - \alpha\,\mathrm{sinc}^2(\pi z)\sin(2\pi z)\right].$$

For the first order FLL here, the dimensionless dynamic stress can be written as ([9], page 389)

$$\gamma_z = \frac{\frac{T_I}{2\pi}\nu}{4B_n} = \frac{\dot{\Delta f}_i\,T_I}{4B_n}, \text{ dimensionless.} \tag{B-4}$$

With γ_z defined in Eq. (B-4) and $\sigma_{\Delta fT_I}^2$ in Eq. (7), α and β can be further represented as

$$\alpha = \frac{1}{2\pi^2\sigma_{\Delta fT_I}^2}, \text{ and} \tag{B-5}$$

$$\beta = \alpha\cdot\frac{2\pi}{T_I}\gamma_z. \tag{B-6}$$

Finally, Eqs. (B-3), (B-4), (B-5), (B-6), and (7) completely define the FPE for the cross-product FLL in the domain of the normalized frequency error. Furthermore, the FPE is in terms of B_n, C/N_0, T_I, normalized initial frequency offset Δf_iT_I, and normalized frequency ramp input $\dot{\Delta f}_i\,T_I$.

REFERENCES

1. Travis, C., "Automatic Frequency Control," *Proc. The Institute of Radio Engineers, Vol. 23, No. 10*, Oct., 1935.
2. Natali, F.D., "AFC Tracking Algorithms," *IEEE Transactions Communications, Vol. COM-32, No. 8*, pp. 935-947, August 1984.
3. Natali, F.D., "Noise Performance of a Cross-Product AFC with Decision Feedback for DPSK Signals," *IEEE Transactions Communications, Vol. COM-34, No. 3*, pp. 303-307, March 1986.
4. Cahn, C.R., "Improving Frequency Acquisition of a Costas Loop," *IEEE Transactions Communications, Vol. COM-25, No. 12*, pp. 1453-1459, December 1977.
5. Chiou, T.Y., Gebre-Egziabher, D. and et al, "Model Analysis on the Performance for an Inertial Aided FLL-Assisted-PLL Carrier-Tracking Loop in the Presence of Ionospheric Scintillation," *Proc. ION NTM 2007.*
6. Haykin, S., Communication Systems, 4th Edition, *John Wiley & Sons, Inc.*, 2001.
7. Ward, P.W., "Satellite Signal Acquisition, Tracking, and Data Demodulation," in *Understanding GPS Principles and Applications, Second Edition, Artech House, Washington, DC, 2006*, pp. 153-241.
8. Viterbi, A.J., Principles of Coherent Communication, *McGraw-Hill Inc.*, 1966
9. Van Dierendonck, A.J., "GPS Receivers," in *Global Positioning System: Theory and Applications, Vol. 1, AIAA, Washington, DC, 1996*, pp. 330-433.
10. Gerald, C.F., and Wheatley, P.O., Applied Numerical Analysis, *5th edition, Addison-Wesley*, pp. 628-650, 1994.
11. Tikhonov, V.I., "The Operation of Phase and Automatic Frequency Control in the Presence of Noise," *Automation and Remote Control, Vol. 21, No.3, AIAA, 1960*, pp. 209-214.
12. Holmes, J.K., Coherent Spread Spectrum Systems, *John Wiley & Sons, Inc.*, 1982.
13. Holmes, J.K., Spread Spectrum Systems for GNSS and Wireless Communications, *Artech House*, 2007.